Synthesis, characterization and photocatalytic activity of Fe-doped Bi_2O_3 nanoparticles

XIAOMIN ZHANG, LI HAN, DEYONG WU*
School of Chemical and Environmental Engineering, Hubei Minzu University, Enshi, Hubei Province, 445000, China

Fe-doped Bi_2O_3 nanoparticles were prepared by the solvothermal method and subsequent calcination process, and characterized by X-ray diffraction (XRD), transmission electron microscopy (TEM), X-ray photoelectron spectroscopy (XPS), photoluminescence (PL) and UV-visible spectroscopy. XPS spectra confirmed the Fe^{3+} ions insert into the matrix interior of Bi_2O_3 nanoparticles. XRD patterns affirmed b-Bi_2O_3 phase did not change after Fe-doping. Compared to the pristine Bi_2O_3, Fe-doped Bi_2O_3 nanoparticles exhibited improved visible-light-driven photocatalytic efficiency for degradation of methyl orange. This result may be attributed to that Fe-doping can effectively improve the utilization of visible light and hinder the recombination process.

(Received January 22, 2019; accepted October 9, 2019)

Keywords: Fe-doping, Bi_2O_3 nanoparticles, Photocatalysis, Substitution

1. Introduction

Nowadays, semiconductor photocatalysis has become a hot research in the field of environmental protection [1-3]. However, due to the wide band gap, the popular semiconductor photocatalysts (TiO_2, ZnO) only respond to the ultraviolet (UV) region of solar light [4,5]. For fully utilizing the solar energy, many kinds of materials with visible light photocatalytic activity have been developed, such as BiOI [6], Bi_2MoO_6 [7], $BiVO_4$ [8]. Bismuth oxide (Bi_2O_3) with a suitable band gap (~2.8 eV) has huge potential in the visible-light-driven photocatalytic applications [9-11]. However, like other pure photocatalyst, Bi_2O_3 also has the problem of the high recombination rate of photogenerated e^-/h^+ pairs. To solve this problem, some effective strategies have been used, such as constructing heterojunctions [12], doping [13], surface modification [14].

Transition metal-doping has been proved as an effective way to improve photocatalytic performance [15,16]. Many metal elements have been applied to enhance the photocatalytic activity of Bi_2O_3, including Zn [17], Ho [18], Fe [19] and Nd [20]. Among these metals, Fe^{3+} ion can form a dopant-induced energy-band and hinder the recombination proces [21-23]. Fe^{3+} ion has been widely applied as a doping metal to improve the photocatalytic activity, and the Fe-doped materials all exhibited a higher photocatalytic activity under visible light irradiation, such as Fe-doped SnS_2 [21], Fe-doped BiOBr [22], Fe-doped BiOI [23]. Meanwhile, β-Bi_2O_3 has a narrower band gap (~2.4 eV) than that of α-Bi_2O_3 (~2.9 eV) [9]. Herein, we prepared Fe-doped β-Bi_2O_3 by the solvothermal method and subsequent calcination process. The characterization of Fe-doped Bi_2O_3 was observed by TEM, XRD, DRS, PL and XPS, and Fe-doped Bi_2O_3 exhibited increased photocatalytic activity in the degradation of MO under visible light irradiation.

2. Experimental

2.1. Preparation of Fe-doped Bi_2O_3 nanoparticles

The reagents and solvents were of analytical reagent grade and used without further purification. Fe-doped Bi_2O_3 nanoparticles were synthesized by a two-step method. Firstly, 10 mmol of Bi $(NO_3)_3.5H_2O$, 10 mmol of glucose and 0.5 mmol of $Fe(NO_3)_3.9H_2O$ were dissolved in 40 mL, 20 mL and 20 mL of ethylene glycol (EG), respectively. After all dissolved, the solutions were mixed together. Then, the mixture was transferred into a 100 mL Teflon-lined stainless steel autoclave, and the solvothermal reaction proceeded at 160 °C for 12 h. The precipitate was collected and washed with deionized water and ethanol for several times, and dried at 80 ^oC in oven. Secondly, the dried product was calcined in a muffle furnace at 300 ^oC for 2 h with a ramp rate of 5 ^oC/min to prepare the Fe-doped Bi_2O_3 sample. For comparison, pure Bi_2O_3 was synthesized by the same process without adding $Fe(NO_3)_3.9H_2O$.

2.2. Characterization

The morphology of the catalyst was observed by transmission electron microscope (TEM, JEOL-100CX, Japan). The crystallinity of powder was characterized by powder X-ray diffraction (XRD, D/max-2200/PC, Rigaku Corporation, Japan) with Cu Ka radiation. XPS experiments were carried out on a RBD upgraded PHI-5000C ESCA system (Perkin Elmer, USA). UV-Vis diffuse reflectance spectra (DRS) of the samples were recorded on a UV-Vis spectrophotometer (TU-1901) with an integrating sphere attachment. The photoluminescence (PL) spectra of the samples were obtained by using a Varian Cary Eclipse spectrometer with an excitation wavelength of 380 nm. The visible light photocatalytic activity of catalyst was evaluated, and the process was described in our previous report [24].

3. Results and discussion

The XRD patterns of the as-prepared Bi_2O_3 and Fe-doped Bi_2O_3 are shown in Fig. 1. All the diffraction peaks are well indexed to β-Bi_2O_3 phase (JCPDS card no. 078-1793) [9]. The main diffracted peaks at 2θ = 28.10°, 31.77°, 32.71°, 46.19°, 47.01°, 54.26°, 55.54°and 57.83°are associated with the (201), (002), (220), (400), (302), (213), (421) and (402) planes. After Fe doping, the phase structure has no obvious change. Meanwhile, other crystalline phases and impurities are not observed. The morphology of Fe-Bi_2O_3 was observed by TEM. As presented in Fig. 2, the Fe-doped Bi_2O_3 nanoparticles are gathered together. The lattice fringe with a spacing of 0.319 nm is ascribed to the (201) plane of β-Bi_2O_3 [25].

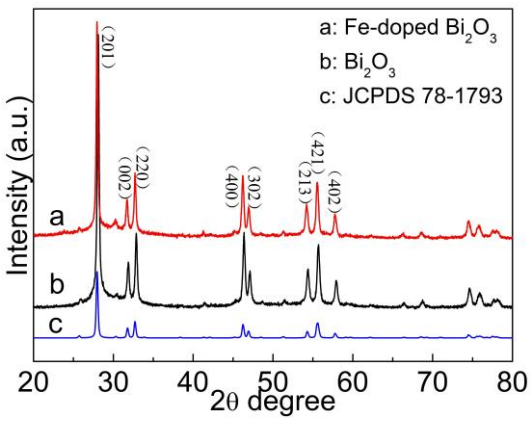

Fig. 1. XRD patterns of the prepared Bi_2O_3 a nd Fe-doped Bi_2O_3

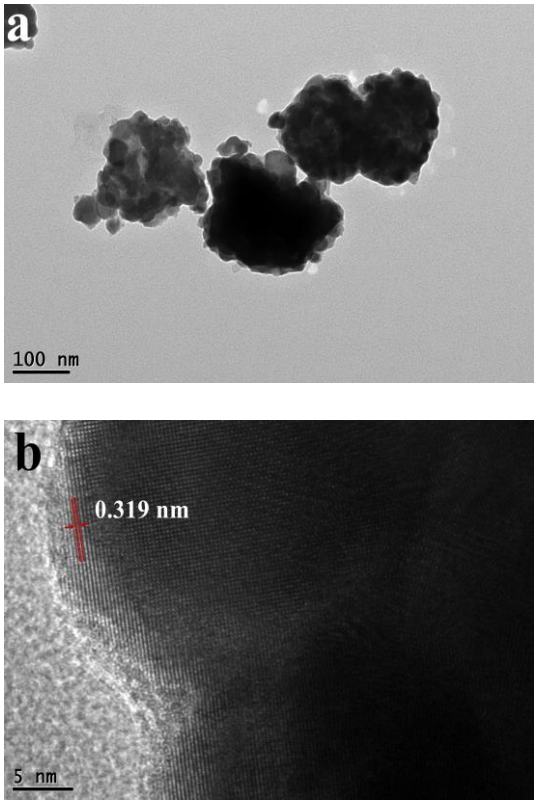

Fig. 2. Low-magnified TEM image (a) and High-resolution TEM image (b) of Fe-doped Bi_2O_3

To investigate the chemical state of the elements, pure Bi_2O_3 and Fe-doped Bi_2O_3 were measured by XPS. As shown in Fig. 3a, two peaks at 724.5 eV and 712.5 eV could be attributed to $2p_{1/2}$ and $2p_{3/2}$ of Fe^{3+} ions. The peak value of $2p_{3/2}$ of Fe^{3+} is different from that in Fe_2O_3 (at 710.7 eV) [26, 27]. The difference is owning to the substitution of Fe^{3+} for Bi^{3+} and the formation of Bi-O-Fe bonds in Fe-doped Bi_2O_3 crystal [26]. The ionic radius of Fe^{3+} (0.065 nm) is smaller than that of Bi^{3+} (0.103 nm), so the Fe^{3+} ions could substitute Bi^{3+} and insert into the matrix interior of Bi_2O_3 crystals. For the Bi 4f XPS spectra (Fig. 3b), there are two peaks, corresponding to Bi $4f_{5/2}$ and Bi $4f_{7/2}$, respectively. The values of Bi $4f_{5/2}$ and Bi $4f_{7/2}$ are 164.33, 159.02 eV in Bi_2O_3, and 164.19, 158.88 eV in Fe-doped Bi_2O_3, respectively. The value difference of 0.14 eV may be attributed to the existence of Bi-O-Fe bonds in Fe-doped Bi_2O_3 crystal. The above results provide indirect evidence that the Fe^{3+} ions were successfully incorporated into Bi_2O_3 crystals.

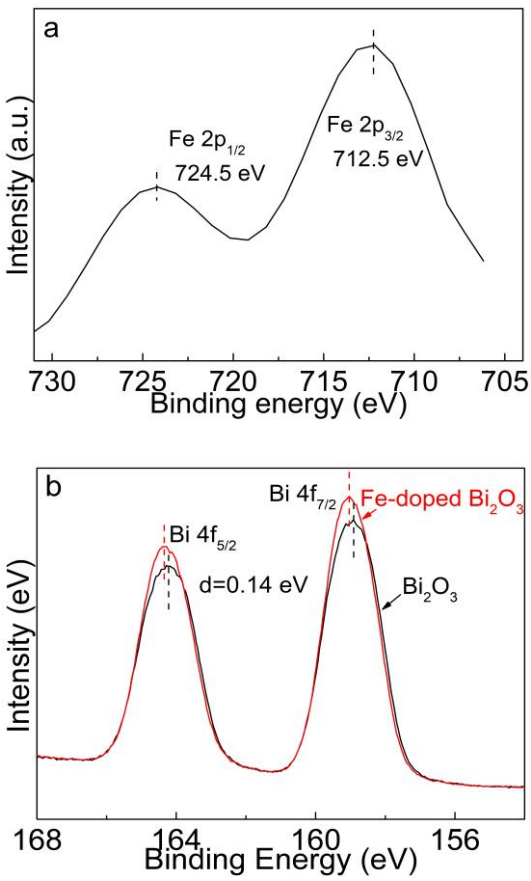

Fig. 3. XPS spectra of Fe-doped Bi_2O_3: Fe 2p (a) and Bi 4f (b)

The optical absorption properties of pure Bi_2O_3 and Fe-doped Bi_2O_3 were characterized by UV-vis spectroscopy. As shown in Fig. 4, pure Bi_2O_3 sample exhibited an absorption edge at around 538 nm, and Fe-doped Bi_2O_3 performed a 581 nm absorption band-edge in the visible light range. Meanwhile, Fe-doped Bi_2O_3 displayed improved light absorption in the UV and visible light range. This phenomenon may be attributed to a d-d transition in the iron species [28].

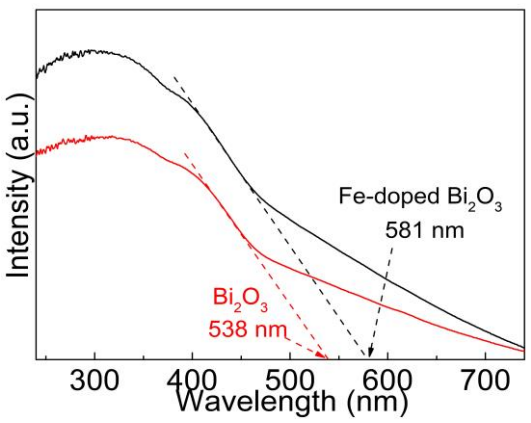

Fig. 4. UV-vis diffuse reflectance spectra of pure Bi_2O_3 and Fe-doped Bi_2O_3

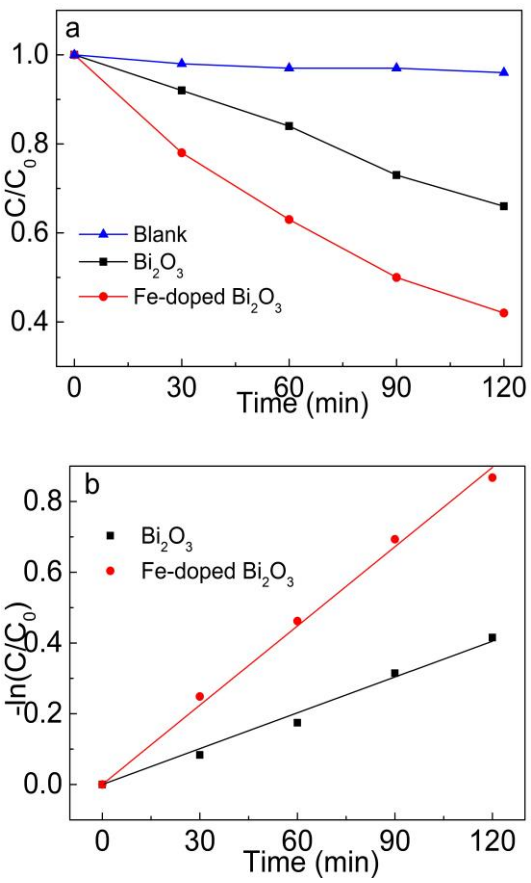

Fig. 5. Photocatalytic activity (a) and kinetic plots (b) of pure Bi_2O_3 and Fe-doped Bi_2O_3 in degradation of MO under visible light irradiation

The photocatalytic activities of pure Bi_2O_3 and Fe-doped Bi_2O_3 were investigated through photodegradation of MO under visible light irradiation (λ>420 nm). As shown in Fig. 5a, MO could not be degraded under visible light irradiation without photocatalyst, pure Bi_2O_3 and Fe-doped Bi_2O_3 can removed about 34% and 63% of MO over 120 min, respectively. Generally, the photocatalytic degradation of pollutants follows pseudo-first-order reaction [29], and its kinetics could be expressed as the formula $\ln(C/C_0) = -k\,t$, where C_0 and C are the initial concentration of MO and the concentration of pollutant at a reaction time of t, respectively, k is the degradation rate constant. Fig. 5b shows the kinetic fitting curves for the MO degradation with different samples. The photocatalytic degradation rates are 0.00338 min^{-1} and 0.00747 min^{-1} for pure Bi_2O_3 and Fe-doped Bi_2O_3, respectively. The degradation rate of Fe-doped Bi_2O_3 is about two times higher than that of pure Bi_2O_3. The enhanced photocatalytic activity of Fe-doped Bi_2O_3 should be attributed to two reasons. On the one hand, Fe-doping narrows the band gap of Bi_2O_3, as shown in Fig. 4, resulting in the superior visible light absorption and the larger numbers of photo-generated e^-/h^+ pairs. On the other

hand, more importantly, the appropriate Fe^{3+} doping benefits the charge separation. Fe^{3+} can turn into Fe^{2+} and Fe^{4+} ions by trapping photo-generated electrons or holes, respectively, which can hinder the recombination process and enhance photocatalytic activity [23,27,30]. Moreover, the PL results (Fig. 6) approved that Fe-doping is good for improving the the charge separation. Comparatively, the PL intensity of Fe-doped Bi_2O_3 particles exhibit a significant decrease, suggesting the lower recombination rate of photo-generated charge carriers [31,32].

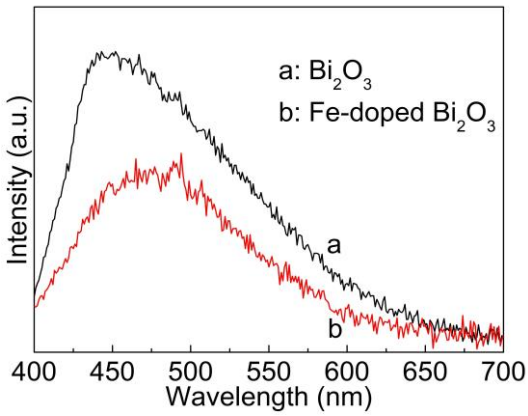

Fig. 6. The photoluminescence spectra of Bi_2O_3 and Fe-doped Bi_2O_3 samples

4. Conclusion

In this work, we successfully prepared β-Bi_2O_3 and Fe-doped β-Bi_2O_3 phtocatalysts by the solvothermal method and subsequent calcination process. XRD results proved Fe-doping has no obvious effect on the crystal structure of β-Bi_2O_3. XPS spectra affirmed that Fe^{3+} ions substitute Bi^{3+} and insert into the matrix interior of Bi_2O_3 crystals. DRS results indicated Fe-doping can improve the utilization of visible light. The absorption edge shifted from 538 nm to 581 nm after Fe doping. PL results certified Fe-doping increase the photo-generated carries separation. Compared to the pristine Bi_2O_3, Fe-doped Bi_2O_3 nanoparticles exhibited enhanced visible-light-driven photocatalytic efficiency for degradation of methyl orange.

Acknowledgments

This project was funded by The National Natural Science Foundation of China (21767009), Undergraduate Innovation Program of Hubei Province (201810517033).

References

[1] P. Lorkit, N. Phatharapeetranun, B. Ksapabutr, S. Wongkasemjit, N. Chaiyut, M. Panapoy, Optoelectron. Adv. Mat. **12**(5-6), 347 (2018).
[2] D. Wu, M. Long, ACS Appl. Mat. Interfaces **3**(12), 4770 (2011).
[3] M. H. Li, Y. B. Liu, L. M. Dong, C. S. Shen, F. Li, M. H. Huang, C. Y. Ma, B. Yang, X. Q. An, W. Sand, Sci. Total Environ. **668**, 966 (2019).
[4] S. Kalpana, S. S. Krishnan, A. Bhaskaran, T. S. Senthil, S. V. Elangovan, Optoelectron. Adv. Mat. **12**(5-6), 353 (2018).
[5] D. Y. Wu, M. C. Long, J. Y. Zhou, W. M. Cai, X. H. Zhu, C. Chen, Y. H. Wu, Surf. Coat. Tech. **203**(24), 3728 (2009).
[6] P. Intaphong, A. Phuruangrat, S. Thongtem, T. Thongtem, Mater. Lett. **213**, 88 (2018).
[7] Y. L. Jia, Y. H. Lin, Y. Ma, W. B. Shi, Mater. Lett. **234**, 83 (2019).
[8] Y. Wang, G. Q. Tan, H. J. Ren, A. Xia, B. Li, D. Zhang, M. Wang, L. Lv, Mater. Lett. **229**, 308 (2018).
[9] G. K. Valencia, A. Lopez, A. Hernandez-Gordillo, R. Zanella, S. E. Rodil, Ceram. Int. **44**(18), 22329 (2018).
[10] J. Chen, J. Zhan, F. H. Ding, Q. H. Li, Y. W. Tang, J. Inorg. Mater. **33**(8), 919 (2018).
[11] X. Xiao, S. H. Tu, C. X. Zheng, H. Zhong, X. X. Zuo, J. M. Nan, RSC Advances **5**(91), 74977 (2015).
[12] Q. Zou, H. Li, Y. P. Yang, Y. C. Miao, Y. N. Huo, Appl. Surf. Sci. **467**, 354 (2019).
[13] H. Sudrajat, S. Hartuti, J. Park, J. Alloys Compd. **748**, 390 (2018).
[14] D. Luo, Y. Kang, Mater. Lett. **233**, 98 (2018).
[15] S. Stojadinovic, N. Tadic, N. Radic, B. Grbic, R. Vasilic, Surf. Coat. Tech. **337**, 279 (2018).
[16] S. Jagadhesan, V. Senthilnathan, T. S. Senthil, Optoelectron. Adv. Mat. **12**(5-6), 360 (2018).
[17] G. Viruthagiri, P. Kannan, N. Shanmugam, Photonic. Nanostruct. **32**, 35 (2018).
[18] N. Prasad, B. Karthikeyan, Appl. Phys. a-Mater. **124**(6), 421 (2018).
[19] G. K. Dinesh, S. Anandan, T. Sivasankar, Environ. Sci. Pollut. R. **23**(20), 20100 (2016).
[20] K. S. Al-Namshah, R. M. Mohamed, Appl. Nanosci. **8**(5), 1233 (2018).
[21] J. Srivind, S. Balamurugan, K. Usharani, D. Prabha, M. Suganya, V. S. Nagarethinam, A. R. Balu, J. Mater. Sci-Mater. El. **29**(11), 9016 (2018).
[22] G. Jiang, X. Wang, Z. Wei, X. Li, X. Xi, R. Hu, B. Tang, R. Wang, S. Wang, T. Wang, W. Chen, J. Mater. Chem. A, **1**(7), 2406 (2013).
[23] M. M. Wang, J. Z. Gao, G. Q. Zhu, N. Li, R. L. Zhu, X. M. Wei, P. Liu, Q. M. Guo, RSC Advances **6**(108), 106615 (2016).
[24] D. Wu, C. Wu, H. Tan, J. Mater. Sci-Mater. El.

29(13), 11090 (2018).
[25] C. F. Yu, P. Y. Yang, L. N. Tie, S. Y. Yang, S. Y. Dong, J. Y. Sun, J. H. Sun, Appl. Surf. Sci. **455**, 8 (2018).
[26] M. C. Gao, D. F. Zhang, X. P. Pu, H. Li, W. Z. Li, X. Shao, D. D. Lv, B. B. Zhang, J. M. Dou, Sep. Purif. Technol. **162**, 114 (2016).
[27] H. Song, Y. Li, Z. Lou, M. Xiao, L. Hu, Z. Ye, L. Zhu, Appl. Catal. B-Environ. **166**, 112 (2015).
[28] C. Regmi, Y. K. Kshetri, T. H. Kim, R. P. Pandey, S. W. Lee, Mol. Catal. **432**, 220 (2017).
[29] D. Wu, M. Long, W. Cai, C. Chen, Y. Wu, J. Alloys Compd. **502**(2), 289 (2010).
[30] C. Han, L. B. Duan, X. R. Zhao, Z. M. Hu, Y. F. Niu, W. C. Geng, J. Alloys Compd. **770**, 854 (2019).
[31] X. L. Zhang, N. Zhang, C. X. Gan, Y. F. Liu, L. Chen, C. Zhang, Y. Z. Fang, Mater. Sci. Semicond. Process. **91**, 212 (2019).
[32] A. Sobhani-Nasab, S. Pourmasoud, F. Ahmadi, M. Wysokowsk, T. Jesionowski, H. Ehrlich, M. Rahimi-Nasrabadi, Mater. Lett. **238**, 159 (2019).

*Corresponding author: wdy001815@126.com